第36卷第1期
2017年2月

红外与毫米波学报
J. Infrared Millim. Waves

Vol. 36, No. 1
February, 2017

文章编号: 1001 - 9014(2017)01 - 0030 - 05

DOI:10.11972/j.issn.1001 - 9014.2017.01.007

Facile design and rapid fabrication of a nearly-square ridge filter

NAN Xue-Li*, ZHANG Bin-Zhen*, CUI Jian-Li, YANG Xin, GE Shao-Lei

(Science and Technology on Electronic Test & Measurement Laboratory,
North University of China, Taiyuan 030051, China)

Abstract: Filters are essential components of communication systems. A rapid and accurate fabrication method is presented in this paper for the design and fabrication of a waveguide filter. The filter was fabricated by using a multi-layer coating and one-time ultraviolet exposure lithography (SU-8 resist on a silicon wafer) to have dimensional fabrication errors of less than 3 μm in height and 1.1° in vertical angle deviation. We demonstrated the feasibility of the proposed class of filters and the fabrication method used and achieved a superior performance (with regard to: insertion loss, return loss, and bandwidth). Consequently the minimum passband insertion loss, which is practically negligible, was measured as being less than 0.5 dB while the return loss is greater than 10 dB during the passband, demonstrating that the chosen rapid fabrication technology is an effective method of terahertz device fabrication. The new technology should become a major driving force forging the future development of terahertz RF devices.

Key words: SU-8 micro-machining, microwave filter, RF MEMS, rectangular waveguide, W band
PACS: 07.10.Cm, 07.57.Kp.

一种近方脊滤波器的设计与快速制造

南雪莉*, 张斌珍*, 崔建利, 杨 昕, 葛少雷
(中北大学 电子测试技术重点实验室,山西 太原 030051)

摘要:滤波器是信号传输系统中的重要组件.提出一种快速、高精度复制工艺方法,用于设计和制备WR-10波段矩形波导滤波器.采用多层匀胶单次紫外曝光工艺(硅片上匀SU-8胶),制备出的滤波器高度误差小于0.03%(3 μm),陡直度误差小于1.1°.实验结果表明,用该方法制备毫米波滤波器技术可行,并取得了卓越的电磁性能(关于:插入损耗,回波损耗和带宽).最终测试结构可知,通带内的插入损耗测得结果小于0.5 dB,几乎可以忽略不计,在整个通带内回拨损耗大于10 dB.结果表明,这种快速制造技术是制备太赫兹射频器件的一种有效办法,这种新技术将成为推动太赫兹射频器件未来发展的主要动力.

关 键 词:SU-8微加工;微波;滤波器;矩形波导;W波段

中图分类号:TN629.1 **文献标识码**:A

Introduction

Terahertz (THz) domain naturally involves a marriage of microwave and optical techniques and thus corresponds to a 3 mm to 30 μm wavelength range[1]. Filters attract much attention due to their efficacy and popularity in communication systems these days, but undoubtedly they are also much more difficult to design and develop in practical applications[2]. Achieving a filter with high frequency, high-Q, and compact size, as well as having low fabrication costs, remains a key challenge[3].

Filters prepared by traditional processing technology cannot be used in aircraft because of their bulk volume and high cost[4]. Traditional metal-milling methods are becoming increasingly difficult, time-consuming, and expensive for filter manufacture[5]. UV photolithographic-

Received date: 2016-11-06, **revised date**: 2016-12-05 **收稿日期**:2016-11-06, **修回日期**:2016-12-05
Foundation items:Supported by National Science Foundation of China (51475438), Research Project Supported by Shanxi Scholarship Council of china (2014-055) and Graduate student education innovation project in Shanxi province (2016BY124)
Biography:NAN Xue-Li (1987-), female, Gansu Dingxi, Ph. D. Research interests are in design and fabrication of MOEMS and RF-MEMS components and systems
* **Corresponding author**:E-mail: nanxueli@yeah.net; zhangbinzhen@nuc.edu.cn

based micro-machining technology has therefore attracted growing attention due to its high-dimensional accuracy, high achievable structural aspect ratio, and its ability to facilitate large-scale, inexpensive production[6] such as is seen in micro-fluidics on a silicon substrate[7], MEMS inertial switches on a metal substrate[8], MEMS filters[9], and in many other areas[10]. Due to its excellent physical and chemical properties, using the UV-LIGA process to fabricate the filter and other high-frequency RF devices has become the norm[11]. There are reports on filters directly prepared using SU-8 photoresist through UV technology. Even so, in the preparation of structures with size being larger than 500 um, multilayer spin-coating and multi-alignment exposure are needed. It is also reported that the filter structure is divided into several layers before fabrication, but this method needs every layer to be aligned and exposed, to form the final microstructure; this is difficult to prepare in layers and signal transmission losses are relatively large. Therefore, it is urgent to propose a method for rapidly preparing miniature filters with excellent performance.

To obtain a more precise preparation method for the desired micro-structure, we use multi-layer coating and a single-step exposure method to prepare the filter. Herein a 100 GHz central frequency of the rectangular waveguide filter has been designed, manufactured, and tested. The key element of the filter was designed to have a double-resonator structure and a nearly-square ridge to achieve a good bandwidth. The waveguide ports were designed to be mutually opposite in direction to achieve a low return loss. The use of this technology provides an easy way for fabricating high-frequency microstructures and ensuring good integration of coupling coefficients. The method allows for rapid fabrication of the filter and thus presents a simple and fast production process.

1　Filter design

The schematic diagram of the basic structure simulation model is shown in Fig. 1(a); the centre frequency and bandwidth of the filter (5.98 × 2.54 × 1.27 mm) are 100 GHz and 5 GHz. The insertion loss of 0.2 dB and return loss of 10 dB during the whole passband were observed, demonstrating that the out of band rejection can meet the design requirements. The corresponding resonance frequency of this cube metal cavity can be calculated using the formula,

$$f = \frac{c\sqrt{\left(\frac{m\pi}{a}\right)^2 + \left(\frac{n\pi}{b}\right)^2 + \left(\frac{p\pi}{c}\right)^2}}{2\pi\sqrt{\varepsilon_r}} \quad , \quad (1)$$

where a, b, c are the three dimensions of the resonator, respectively. In this paper, $a = b = c = w = l = 1.05$ mm.

As shown in Fig. 1(b), waveguide is set for a nearly-square waveguide. There is a pair of orthogonal mode of electric field in the waveguide cavity. The corresponding electric field polarization directions are shown in Fig. 1(b) as E_1 and E_2. The angle between the flat ridge and the orthogonal electric field is 45 degrees, and a new electric field is generated by the interference of the orthogonal electric field.

The coupling coefficient of the two modes can be obtained by the follow formula:

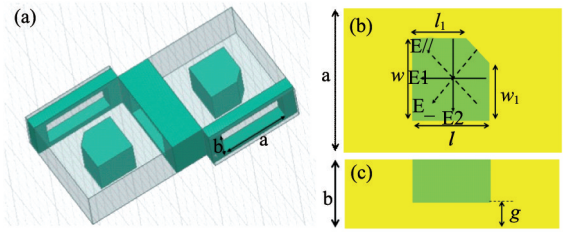

Fig. 1　HFSS 3-d model of a rectangular waveguide filter using two nearly-square ridge resonators. (a) Schematic diagram of the basic structure of the filter. (b) Top views of the resonator and a cross section of rectangular waveguide with flat back. (c) Side views of the resonator. Key dimensions of the filter include: a = 1.85 mm; b = 0.9 mm; $w = l$ = 1.05 mm; $w_1 = l_1$ = 0.775 mm; and g = 0.2 mm

图 1　近方脊波导滤波器 HFSS 三维模型. (a)滤波器的基本结构示意图. (b)谐振器横截面电磁波传输的示意图. (c)谐振器的侧视图. 该滤波器的关键方面包括: a = 1.85 mm; b = 0.9 mm; $w = l$ = 1.05mm; $w_1 = l_1$ = 0.775 mm; and g = 0.2 mm

$$k = \frac{f_2^2 - f_1^2}{f_2^2 + f_1^2} \quad , \quad (2)$$

Where, f_1 *and* f_2 are the resonance frequency of the two patterns, corresponding to the two peaks of the S_{11} parameters.

Two nearly-square ridge resonators were placed in the main mode of rectangular waveguide transmission to support the fundamental TE_{10} mode with $w/l = 1$ (w is ridge width and l the length). The corresponding width and height of the waveguide were designed to be that of a standard WR-10 (2.54 mm and 1.27 mm) waveguide, as shown in Figs. 1(b) and 1(c) (top and side views of the resonator, respectively). The parameters were such that:

$$a < \lambda < 2a \quad \lambda > 2b \quad . \quad (3)$$

The central frequency f is 100 GHz, meeting the conditions for single mode transmission. The ridge resonator has a side length $w = l$ = 1.05 mm, the corner cutting edge length is 0.3889 mm, the gap g is 0.2 mm, and the input/output coupling window is 1.85 mm wide and 1 mm thick. The ridge resonator is the critical component of the dual-mode waveguide structure as the EM field is confined mainly to the ridge gap. The ridge lies between the resonator and the waveguide width side. When the gap g is set to a certain value, there will be a clearance between the two orthogonal degenerate modes.

The nearly-square resonator can be excited in the gap along the length of the resonator (vertical to the die) and across the width (transverse mode) giving two quasi-TEM modes. Mode degeneracy is therefore obtained without increasing the dimensions of the rectangular waveguide housing. As long as the multiple ridge resonators achieve appropriate connections, we can form a compact dual-mode waveguide filter.

Accordingly, when the two square ridge resonator is placed in the 90° C H-plane bend of a standard WR-10 waveguide (Fig. 2a), the latter being coupled to the other orthogonal mode through the chamfered corner, the resulting coupling scheme produces dual-mode behaviour.

The cavity mode and coupling topology are shown in Fig. 2b, where the source S and the load L represent the fundamental TE_{10} mode in the input and output sections[12]. The longitudinal resonant modes are expressed using "1" and "4", and the transverse resonant modes are expressed using "2" and "3". The coupling coefficient M within the filter is determined by the size of the cut-away corner on the square ridge resonator and its relative location. The individually designed ridge resonators are excited by the main TE_{10} mode. Subtle optimisation of the overall structure is still necessary to compensate for any additional spurious coupling occurring between the ridge resonators.

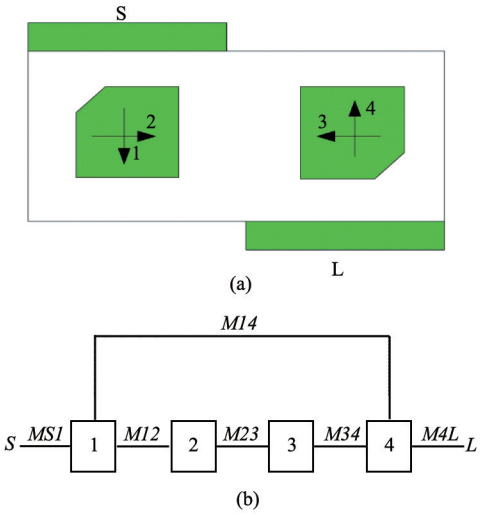

Fig. 2 Schematic diagram of the coupling mode in the filter cavity and the coupling topology. (a) Nearly-square ridge resonators in the rectangular waveguide and the coupling modes. (b) The coupling topology

图 2 滤波器谐振腔耦合模式及耦合拓扑结构示意图. (a) 矩形波导中的近方脊谐振器及其耦合模;(b)耦合拓扑图

2 Fabrication details

Primary processing steps for the W band waveguide filters are shown in Fig. 3.

Briefly, a 2-inch p-type silicon wafer, used as the substrate, was cleaned by acetone, isopropyl, alcohol (IPA), and DI water sequentially in an ultrasonic bath for 5 min, respectively. After dehydration on a hotplate at 100 °C for about 10 min, SU-8 2100 photoresist was spin-coated on the wafer to obtain an 800 μm-thick SU-8 layer. The second layer of SU-8 was then spin-coated at 1500 rpm for 30 s to obtain a 205 μm thick layer. The third 220-μm thick resist layer was also formed by the same process. It was then exposed under a suitable UV exposure dosage. Finally, the sample on the silicon wafer was twice-immersed in SU-8 developer in an ultrasonic cleaning machine, while being stirred, to ensure sufficient development.

After cleaning, the samples were then blow-dried and loaded into a vacuum chamber for metallisation. A 308R evaporator was used for metallisation, which started with oxygen plasma cleaning for 30 s, and finally a

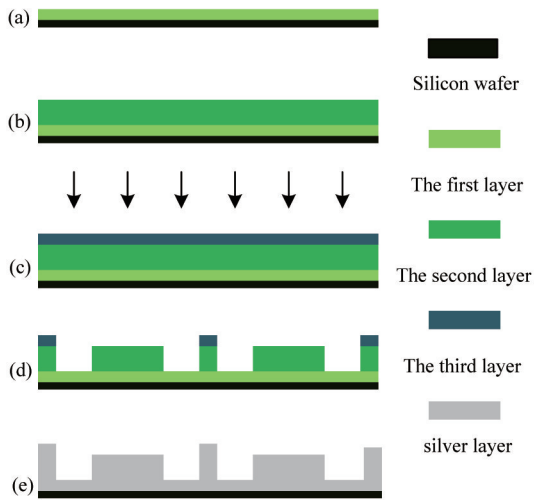

Fig. 3 Fabrication details of the waveguide filter. (a) Silicon wafer cleaning and spinning of SU-8 2100 thereon. (b) Coating the second layer of SU-8 photoresist. (c) Coating third layer of SU-8 photoresist and exposure. (d) Development and post-bake treatment. (e) Sputtering silver on the surface of cured three-layer SU-8 resist

图 3 滤波器详细制备工艺流程图. (a)清洗硅片然后在硅片上匀 SU-8 2100 胶;(b) 匀第二层 SU-8 2100 胶;(c) 匀第三层 SU-8 2100 胶及紫外曝光;(d)显影及后烘;(e)在固化后的 SU-8 胶表面沉积一层银层

1 μm-thick silver layer was thermally evaporated onto the surface of the filter. The sample holder rotated continuously at a tilted angle to coat all sidewalls. Since silver has a high electrical conductivity, it was used to form the metallic layer. Because of its high conductivity (6.3×10^7 S/m, for an electromagnetic wave of 100 GHz), the required skin depth of the silver film was calculated to be about 198.23 nm. We choose the sputtering silver thickness (2 μm), which is more than five times higher than the skin depth at its centre frequency of 100 GHz. This thickness ensures that it does not produce significant additional insertion loss.

The final filter structure, with its silver layer, is shown in Fig. 4a, while the SEM image is shown in Fig. 4b where the sidewall quality of the filter is seen to be excellent. Using a laser confocal microscope, the vertical angle was found to be 88.9°(Fig. 4c), which represented a deviation of 1.1° from the ideal value of 90° with respect to the wafer surface.

3 Measurements and results

During measurement, the fabricated filter and the waveguide section were placed in the middle of two standard WR-10 waveguide flanges (type UG-387). The filter was designed to have a central frequency, bandwidth, insertion loss, and return loss of 100 GHz, 5 GHz, 0 dB, and 10 dB, respectively. The simulated and measured results of the S parameters for the W-band filter are shown in Fig. 5. For intuitive comparison of the experimentally measured and simulated results, they are plotted together.

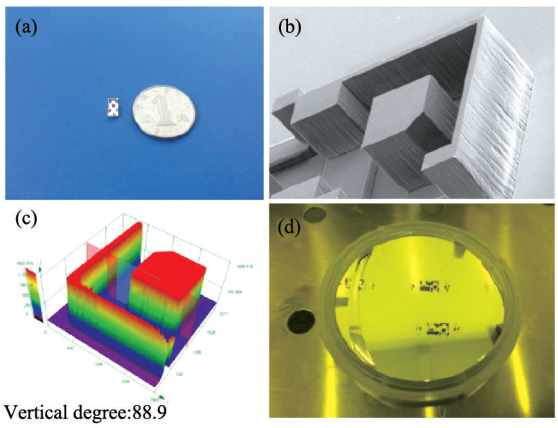

Fig. 4　SEM and confocal microscope images of the prototype waveguide filter. (a) The fabricated filter. (b) SEM image. (c) Confocal microscope image showing the verticality of the sidewalls (d) sample drawing
图 4　波导滤波器电子显微镜图及共聚焦显微镜图. (a)制备获得的滤波器 (b)电子显微镜 SEM 图 (c)共聚焦显微镜侧壁陡直度测试图 (d)样品图

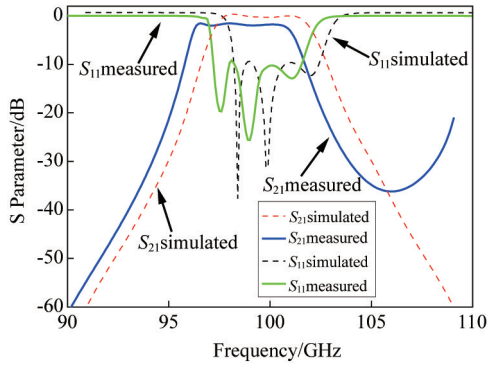

Fig. 5　Measurement and simulation results for the WR-10 band rectangular waveguide dual-mode waveguide filter with two nearly-square ridges
图 5　双模脊波导滤波器的仿真与测试结果图

Compared with the simulated results, the insertion loss was measured at 0.5 dB, return loss was better than 10 dB during the passband, and the out-band rejection at high frequencies was much higher than at low frequencies. This is because the sample and the test equipment were aligned with the groove on the flange plate, which was difficult to realize the seamless connection with the standard waveguide. This can also lead to error on the out-band rejection, which will effect the high frequency segment. After removing the unavoidable effects of the errors in the test instruments and transmission line, the small remaining difference may be attributable to the rough internal surface. The rough surface increases the metal layer conduction losses.

As we all know, the measured frequency shift occurs in the centre frequency compared with that simulated. This difference is due to processing precision in the square ridge and waveguide cavities. In order to better illustrate the problem, we have made a comparison of the latest filter performance in recent years. The specific comparison results are illustrated in Table 1.

By comparing the data in Table 1, it can be found that the fabricated filters in this paper show good conformity with the maximal error being 0.3% (there was a 3% difference between the fabricated dimensions and the design dimensions). Therefore, the production process slightly influences the key sizes of the cavity filters, including the size of the resonant cavities and the width of the sidewall. The precise fabrication was realized without influencing the electromagnetic performance of filters including centre frequency, bandwidth, insertion loss, and return loss. So, to obtain a better structure, the precision of the preparation process plays a crucial role and the fabrication tolerance in the initial design of the mask needs to be taken into consideration.

Table 1　Comparison of electromagnetic properties and fabrication error of different filters
表 1　不同滤波器电磁性能及制备精度的比较

Performance parameter	Xiaobang Shang[13]	X. H. Zhao[5]	Zhang Chen[1]	Junping Duan[14]	This filter
Insertion loss	1 dB	2 dB	2 dB	0.8 dB	0.5 dB
Return loss	10 dB	15 dB	20 dB	15 dB	30 dB
Central frequency	300 GHz	174 GHz	350 GHz	100 GHz	100 GHz
Bandwidth	3 GHz	9.6 GHz	30 GHz	3 GHz	5 GHz
Shifted	7 GHz	4 GHz	6 GHz	3 GHz	1 GHz
Fabrication errors	6%	4%	5%	5%	3%

4　Conclusions

A compact, robust W-band waveguide filter has been devised, manufactured, and tested. The waveguide ports were designed to be mutually opposed in direction to achieve a decent bandwidth and return loss. The filter was fabricated by multi-layer coating and one-time ultraviolet exposure lithography (SU-8 resist on silicon wafer). Implementing miniaturisation of the product shortened the production cycle. The measured central frequency of the dual-mode filter only downshifted by around 1 GHz due to the fabrication tolerances imposed. It was found that the measured parameters of the filter agreed with the simulated results. This fabrication method can further improve fabrication accuracy and improve the electromagnetic performance of THz, and higher-frequency band RF devices.

Acknowledgment

This research was supported by the National Natural Science Foundation of China (Grant no. 51475438), Research Project Supported by Shanxi Scholarship Council of china (Grant no. 2014-055) and Graduate student education innovation project in Shanxi province (Grant no. 2016BY124). The experimental work was conducted at State Science and Technology Electronic Test and Measurement Laboratory of The North University of China and The State Key Laboratory for Manufacturing System Engineering of Xi'an Jiao Tong University of China.

References

[1] Chen Z, Zheng Y, Kang X, *et al*. WR-2.8 band micromachined rec-

tangular waveguide filter [J]. *Journal of Infrared, Millimeter, and Terahertz Waves*, 2013, **34**(12): 847-855.
[2] Hu R, Liang Y, Qian S, *et al.* Dual-band bandpass filter based on compound metallic grating waveguide structure [J]. *Optics Communications*, 2015(336): 110-115.
[3] cSimcsek S, Topuz E, Niver E. A novel design method for electromagnetic bandgap based waveguide filters with periodic dielectric loading [J]. *AEU-International Journal of Electronics and Communications*, 2012, **66**(3):228-234.
[4] Bao X, Dargent T, Cattan E. Micromachining SU-8 pivot structures using AZ photoresist as direct sacrificial layers for a large wing displacement [J]. *Journal of Micromechanics and Microengineering*, 2010, **20**(2): 025005.
[5] Zhao X H, Bao J F, Shan G C, *et al.* D-band micromachined silicon rectangular waveguide filter [J]. *Microwave and Wireless Components Letters, IEEE*, 2012, **22**(5): 230-232.
[6] Shao G, Qiu W, Wang W. Fast replication of out-of-plane microlens with polydimethylsiloxane and curable polymer (NOA73) [J]. *Microsystem Technologies*, 2010, **16**(8): 1471-1477.
[7] Yang L, Hao X, Wang C, *et al.* Rapid and low cost replication of complex microfluidic structures with PDMS double casting technology [J]. *Microsystem Technologies*, 2014, **20**(10): 1933-1940.
[8] Du L, Zhao M, Wang A, *et al.* Fabrication of novel MEMS inertial switch with six layers on a metal substrate [J]. *Microsystem Technologies*, 2014: 1-8.
[9] Zhang Y, Zhuang Y, Li Z, *et al.* A 5-bit lumped 0.18-μm CMOS step attenuator with low insertion loss and low phase distortion in 3-22 GHz applications [J]. *Microelectronics Journal*, 2014, **45**(4): 468-476.
[10] Wang L, Xiong Y-Z, Zhang B, *et al.* 0.7-dB Insertion-Loss D-Band Lange Coupler Design and Characterization in 0.13 μm SiGe BiCMOS Technology [J]. *Journal of Infrared, Millimeter, and Terahertz Waves*, 2010, **31**(10): 1136-1145.
[11] Abgrall P, Conedera V, Camon H, *et al.* SU-8 as a structural material for labs-on-chips and microelectromechanical systems [J]. *Electrophoresis*, 2007, **28**(24): 4539-4551.
[12] Kumar S, Kumari A, Pradhan B. Analysis of evanescent field of TE and TM mode in the grounded slab metamaterial waveguide structure [J]. *Optik-International Journal for Light and Electron Optics*, 2015, **126**(23): 3706-3712.

(上接9页)

decrease the parasitical source/drain resistance, the source-to-drain distance (L_{sd}) was scaled to 600 nm using MOCVD to regrow n^+-GaN Ohmic contacts. In addition, a 50 nm rectangular gate was fabricated by self-aligned-gate technology in the middle of the source and drain. Due to the scaled source-to-drain distance, the InAlN/GaN HFET showed a high I_{ds} of 2.11 A/mm @ $V_{gs}=1$ V and a peak g_m of 609 mS/mm. On-wafer small-signal RF measurements indicate that the values of extrapolated f_T and f_{max} for the device were 220 GHz and 48 GHz, respectively. To our best knowledge, the extrapolated value of f_T is the best domestic reported one for InAlN/GaN HFETs.

References

[1] GONSCHOREK M, CARLIN J F, GRANDJE-AN N, *et al.* Two-dimensional electron gas dens-ity in $Al_{1-x}In_xN$/AlN/GaN heterostructures ($0.03 \leqslant x \leqslant 0.23$) [J]. *Journal of Applied Physics*, 2008, **103**: 093714(1-5).
[2] MIZUTANI T, ITO M, KISHIMOTO S, AlGaN/ GaN HEMTs with thin InGaN cap layer for normally off operation [J]. *IEEE Electron Device Letters*, 2007, **28**(7):549-551.
[3] Pei Y, POBLENZ C, CORDON A L, *et al.* X-and Ka-band power performance of AlGaN/ GaN HEMTs grown by ammonia-MBE [J]. *IEEE Electroics Letters*, 2008, **44**(9): 598-599.
[4] MICOVIC M, KURDOGHLIAN A, BROWN D F, *et al.* 92-96 GHz GaN power amplifiers [C]. IEEE MTT-S International, Canada, 2012: 1-3.
[5] BROWN D F, A WILLIAMS, SHINOHARA K, *et al.* W-band power performance of AlGaN/ GaN DHFETs with regrown n^+ GaN ohmic contacts by MBE [C]. IEEE Electron Devices Meeting (IEDM), Washington, 2011: 19.3.1-19.3.4.
[6] KHAN M A, Chen Q, Sun C J, *et al.* Enhance-ment and depletion mode GaN/AlGaN hetero-structure field effect transistors [J]. *Applied Physics Letters*, 1996, **68**(4): 514-516.
[7] CHUNG J W, HOKE W E, CHUMBES E M, *et al.* AlGaN/GaN HEMT With 300-GHz [J]. *IEEE Electron Device Letters*, 2010, **31**(3):195-197.
[8] KUZMÍK J., Power electronics on InAlN/(In)-GaN: Prospect for a record performance [J]. *IEEE Electron Device Letters*, 2001, **22**:510-512.
[9] SUN H, ALT A R, BENEDICKTER H, *et al.* 205 GHz (Al,In)N/GaN HEMTs [J]. *IEEE Electron Device Letters*, 2010, **31**:293-295.
[10] SUN H, ALT A R, BENEDICKTER H, *et al.* 205-GHz (Al,In)N/GaN HEMTs [J]. *IEEE Electron Device Letters*, 2010, **31**(9):957-959.
[11] LEE D S, CHUNG J W, WANG H, *et al.* 245-GHz InAlN/GaN HEMTs with oxygen plasma treat-ment [J]. *IEEE Electron Device Letters*, 2011, **32**:755-757.
[12] LEE D S, GAO X, GUO S, *et al.* 300-GHz InAlN/ GaN HEMTs with InGaN back barrier [J]. *IEEE Electron Device Letters*, 2011, **32**: 1525-1527.
[13] Yue Y, Hu Z, Guo J, *et al.* Ultrascaled InAlN/ GaN High Electron Mobility Transistors with Cutoff Frequency of 400 GHz [J]. *Japanese Journal of Applied Physics*, 2013, **52**(8): 279-287.
[14] Han T T, Dun S B, Lv Y J, *et al.* 70-nm-Gated InAlN/GaN HEMTs Grown on SiC Substrate with $f_T/f_{max}>160$ GHz [J]. *Journal of Semiconductors*, 2016, accepted to be published.
[15] SHINOHARA K, REGAN D, CORRION A, *et al.* Self-aligned-gate GaN-HEMTs with heavily doped n^+-GaN ohmic contacts to 2DEG [C]. IEEE International Electron Devices Meeting, 2012, **48**(11): 27.2.1-27.2.4.
[16] Guo H Y, Lv Y J, Gu G D, *et al.* High Frequen-cy AlGaN/GaN High Electron Mobility Transi-stors with Regrown Ohmic Contacts by Metal Organic Chemical Vapor Deposition [J]. *Chin-ese Physics Letters*, 2015, **32**:118501 (1-3).
[17] CHEN G, KUMAR V, SCHWINDT R S, *et al.* Low Gate Bias Model Extraction Technique for AlGaN/ GaN HEMTs [J]. *IEEE Trans Micro Theory Tech*, 2006, **54**: 2949-2953.
[18] ARDARAVI ĖIUS L, MATULIONIS A, LIBE-RIS J, *et al.* Electron drift velocity in AlGaN/ GaN channel at high electric fields [J]. *Journal of Applied Physics*, 2009, **106**(7): 073708(1-5).